

# Coherent Forward Scattering: A smoking gun of Anderson metal-insulator transitions

Sanjib Ghosh,<sup>1,2,3</sup> Christian Miniatura,<sup>2,1,4,5,6</sup> Nicolas Cherroret,<sup>3</sup> and Dominique Delande<sup>3</sup>

<sup>1</sup>Centre for Quantum Technologies, National University of Singapore, 3 Science Drive 2, Singapore 117543, Singapore

<sup>2</sup>MajuLab, UMI 3654, CNRS-UNS-NUS-NTU International Joint Research Unit, Singapore

<sup>3</sup>Laboratoire Kastler Brossel, UPMC-Sorbonne Universités, CNRS,

ENS-PSL Research University, Collège de France, 4 Place Jussieu, 75005 Paris, France

<sup>4</sup>Department of Physics, National University of Singapore, 2 Science Drive 3, Singapore 117542, Singapore

<sup>5</sup>School of Physical and Mathematical Sciences, Nanyang Technological University, Singapore 637371, Singapore

<sup>6</sup>Université Côte d'Azur, CNRS, INLN; 1361 route des Lucioles, 06560 Valbonne, France

We show that the coherent forward scattering (CFS) interference peak amplitude sharply jumps from zero to a finite value upon crossing a metal-insulator transition. Extensive numerical simulations demonstrate that the CFS peak contrast obeys the one-parameter scaling hypothesis, gives access to the critical exponents of the transition and provides valuable information on the multifractal character of the eigenfunctions at the critical point. These properties make the CFS peak a natural critical quantity and an experimentally observable order parameter of Anderson metal-insulator transitions.

PACS numbers: 05.60.Gg, 72.15.Rn, 42.25.Dd, 03.75.-b

Nearly sixty years ago, P. W. Anderson showed that interference can completely suppress the diffusion of a quantum particle in a random potential [1]. A deep insight came later with the scaling theory of localization [2, 3]. Relying on a one-parameter scaling hypothesis, it predicted a genuine disorder-driven metal-insulator transition (MIT) for three-dimensional (3D) disordered systems. Since then, various classes of Anderson MITs, with different critical properties, have been identified [4, 5]. Generically, a MIT features a mobility edge separating a metallic phase where waves are extended and propagate diffusively from an insulating phase where waves are localized and diffusive transport is suppressed. Direct experimental proofs of MITs are scarce or elusive because difficult to achieve [6–8]. For instance, if Anderson localization in the orthogonal class has been observed recently with classical waves [9–11] and cold atoms [12, 13], conclusive experiments for the unitary or symplectic classes are still lacking. Furthermore, many questions and controversies remain open. In the context of cold atoms, reported experimental values of the mobility edge [14] differ from theoretical predictions [15] and the critical properties of Anderson MITs, including multifractality [16], have been little studied in actual experiments [17].

So far, one has tracked imprints of Anderson localization on usual transport properties like an anomalous temperature or magnetic field dependence of the conductivity in electronic systems [6], an exponentially small optical transmission [18], large intensity fluctuations [19], deviations from diffusion theory [20] in classical wave systems, or the freezing of a diffusively spreading wave packet in cold atomic systems [13]. But if one aims at a full experimental characterization of an Anderson MIT, then a genuine order parameter is required, i.e. a reliable and measurable critical quantity which is nonzero on one side of the transition and vanishes on the other side.

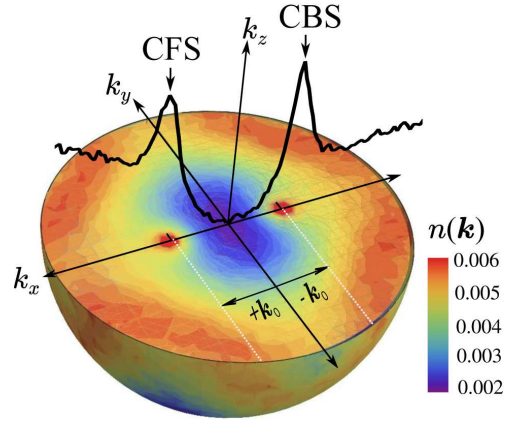


FIG. 1. (Color online) Energy-filtered, disorder-averaged momentum distribution obtained in the insulating regime of the cubic 3D Anderson model (lattice constant  $a$ , tunneling rate  $J$ ) when an initial plane wave  $|\mathbf{k}_0\rangle$  is numerically propagated up to time  $t = 8000\hbar/J$ . The disorder strength is  $W = 20J$ , the energy  $E = J$  and  $\mathbf{k}_0 = \pi/(3a)\hat{e}_x$ . The CFS and CBS peaks are visible at  $\mathbf{k}_0$  and  $-\mathbf{k}_0$  respectively. The solid curve is a cut along  $k_x$ .

In this Letter, we numerically demonstrate that the so-called coherent forward scattering (CFS) peak can play this role. CFS is a robust interference effect triggering a macroscopic peak in the forward direction of the momentum distribution obtained from the evolution of an initial plane wave through a bulk disordered system [21–23]. It resembles the well-known coherent backscattering (CBS) effect which arises due to the pair interference of time-reversed scattering sequences and yields a peak in the backward direction. However, there are fundamental differences between the two effects. Indeed, the CBS peak exists on both sides of the Anderson MIT and shows no discontinuity at the mobility edge [24]. Moreover, the CBS interference relies on time-reversal symmetry and

is absent in systems breaking reciprocity [25]. In contrast, CFS *requires* Anderson localization (it is absent in the metallic phase) and is present in systems where time-reversal invariance is broken [26]. These properties naturally propound CFS as a generic tool to study Anderson MITs. In this Letter, we numerically investigate the CFS properties in the 3D Anderson model [27]. In short, we find that the CFS peak (i) jumps from zero (in the metallic phase) to a finite value (in the insulating phase) when crossing the transition, (ii) obeys the one-parameter scaling hypothesis, (iii) gives access to the critical exponents of the transition and (iv) provides information on the multifractal character of eigenstates at the critical point.

In Fig. 1 we show a density plot of the momentum distribution resulting from the numerical propagation over long times of an initial plane wave  $|\mathbf{k}_0\rangle$  in a 3D random potential. In the insulating phase of the system, we observe two vivid interference peaks, the CBS peak (centered at  $\mathbf{k} = -\mathbf{k}_0$ ) and the CFS peak (at  $\mathbf{k} = +\mathbf{k}_0$ ), sitting on top of a smooth background. For these simulations (and the subsequent ones), we use the Anderson model, with Hamiltonian  $\hat{H} = -J \sum_{\langle ij \rangle} c_i^\dagger c_j + \sum_i V_i c_i^\dagger c_i$ , where lattice sites  $i$  and  $j$  run over a simple 3D cubic lattice comprising  $M^3 = 120^3$  sites with spacing  $a$ . Hopping (of strength  $J$ ) is between nearest-neighbor sites only, and the onsite potential energies  $V_i$  are independent random variables uniformly distributed over  $[-W/2, W/2]$  ( $W$  is the disorder strength). We study the Anderson MIT of this model, following the most accurate known numerical results [28] by fixing the energy  $E = J$  and varying the disorder strength around the critical point  $W_c(E) \approx 16.53J$ . Here and in all simulations reported below, the size of the system ( $M = 120$ ) is much larger than the distance travelled during the propagation time, so that the system is virtually infinite.

Because the initial plane wave covers a wide range of energies with different  $W_c$ , we choose to remove the undesirable energy components by applying the filtering operator  $F_\sigma(E) = \exp[-(E - \hat{H})^2/2\sigma^2]$  onto the initial plane-wave state  $|\mathbf{k}_0\rangle$ . The width of the filter is chosen as  $\sigma = 0.5J$ , so that  $W_c$  is almost independent of energy in the selected range. We then evolve this filtered state with  $\mathcal{U}(t) = \exp(-i\hat{H}t/\hbar)$ . We repeat this computation scheme for 6000 different disorder configurations and calculate the disorder-average momentum distribution  $n(\mathbf{k}, t) = |\langle \mathbf{k} | \mathcal{U}(t) F_\sigma(E) | \mathbf{k}_0 \rangle|^2$ , which is plotted in Fig. 1.

We now investigate how these peaks behave across the Anderson MIT. As found in [29], the CBS peak becomes sizable after a few mean free times  $\tau$ . This occurs whatever  $W$ , the peak amplitude showing *no discontinuity* as the MIT is crossed. The situation is very different for the CFS peak. In the metallic regime  $W < W_c$ , a small CFS peak appears after a few  $\tau$ , but then rapidly dies off. In the insulating regime  $W > W_c$ , in contrast,

the CFS peak becomes sizable over a time scale set by the Heisenberg time  $\tau_H \gg \tau$  (inverse of the mean level spacing within a localization volume, see also below): its amplitude converges in time to the CBS peak value and then stays stationary [22]. In other words, localization triggers a macroscopic CFS peak, which is thus *discontinuous* across the MIT.

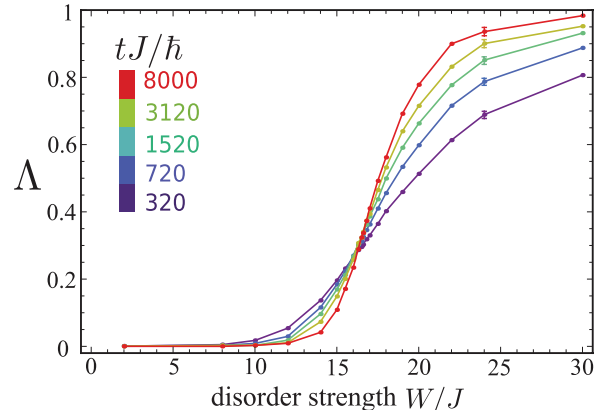


FIG. 2. (Color online) Normalized CFS contrast  $\Lambda$  at energy  $E = J$  as a function of  $W$ , for different propagation times. As time grows from  $t = 320\hbar/J$  to  $t = 8000\hbar/J$ ,  $\Lambda(W)$  converges toward a step function. All curves cross at  $W \approx 16.5J$ , marking the critical point  $W_c$  of the Anderson MIT. The corresponding contrast  $\Lambda_c \approx 0.33$  is time-independent.

We introduce the CFS contrast  $C_F(W, t)$  at  $+\mathbf{k}_0$  and the CBS contrast  $C_B(W, t)$  at  $-\mathbf{k}_0$ . Both are defined as the ratio of the peak height above the background to the background [23]. Because these ratios are rather sensitive to statistical fluctuations of the background, we use the normalized CFS contrast  $\Lambda(W, t) = C_F/C_B$  instead of simply  $C_F$ . In Fig. 2, we show  $\Lambda(W, t)$  as the function of  $W$  for different times ranging from  $t = 320\hbar/J$  to  $t = 8000\hbar/J$ . The observed step is steeper as time increases, as expected for the behavior of an order parameter across a phase transition where time plays the role of the system size. At long times,  $\Lambda$  is 0 in the metallic regime and jumps to 1 in the insulating regime, irrespective of the exact value of  $W$  chosen in each regime. Fig. 2 also shows that all curves cross at  $W \approx 16.5J$ , the critical point  $W_c$  of the MIT. This important result implies that, exactly at the critical point,  $\Lambda(W_c) \equiv \Lambda_c \approx 0.33$  is *time independent*. The meaning of this value will be elucidated later. In the metallic phase, the long-time dynamics of the CFS peak can be captured by diagrammatic techniques [21, 23, 26]. Within this perturbative approach, the CFS is described by a sum of two interference contributions, one featuring a concatenation of two maximally-crossed diagram series and the other being its time-reversed counterpart. We find:

$$\Lambda(W, t) \sim \frac{1}{2\pi\hbar\rho D\sqrt{Dt}} \quad (W < W_c) \quad (1)$$

where  $\rho$  is the disorder-averaged density of states per unit volume (DOS) and  $D$  the diffusion constant. Fig. 3 confirms that the time decay of  $\Lambda(W, t)$  in the metallic regime is indeed well described by a  $1/\sqrt{t}$  dependence, validating Eq. (1) at long times and the fact that  $\Lambda(W, t \rightarrow \infty) = 0$  in the metallic phase.

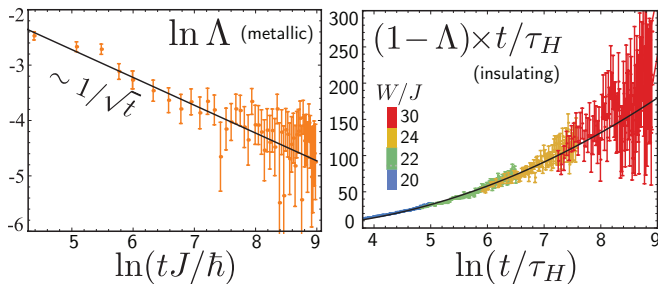


FIG. 3. (Color online) Time dependence of the normalized CFS contrast  $\Lambda(W, t)$  in the metallic (left) and insulating (right) phases. Left: the numerical points are well fitted by  $1/\sqrt{t}$  (solid curve), in agreement with the theoretical prediction Eq. (1). Right: plot of  $(1 - \Lambda)t/\tau_H$  for various  $W > W_c$ . The theoretical prediction (5), obtained in the limit  $t \gg \tau_H$ , is confirmed with  $\alpha = 3.72$  and  $\eta = 0.129$  (solid curve). Here the Heisenberg time  $\tau_H$  has been computed independently by using the dynamics of the CBS peak width [29].

In the insulating phase, the long-time dynamics of the CFS peak cannot be captured by perturbation theory. It is then convenient to expand the initial state  $|\mathbf{k}_0\rangle$  on the eigenstates  $|\varphi_n\rangle$  (energy  $\epsilon_n$ ) of the Hamiltonian. Forgetting for a while the energy filtering, we obtain

$$n(\mathbf{k}, t) = \overline{\sum_{n,m} \varphi_n^*(\mathbf{k}_0) \varphi_n(\mathbf{k}) \varphi_m(\mathbf{k}_0) \varphi_m^*(\mathbf{k}) e^{-i(\epsilon_n - \epsilon_m)t/\hbar}} \quad (2)$$

In the long time limit, the off-diagonal terms  $n \neq m$  give oscillatory contributions which average to 0, so that:

$$n(\mathbf{k}, t \rightarrow \infty) = \overline{\sum_n |\varphi_n(\mathbf{k}_0)|^2 |\varphi_n(\mathbf{k})|^2}. \quad (3)$$

In the insulating phase, the localized eigenstates of our time-reversal invariant system can be chosen real in configuration space, and thus  $\varphi_n(-\mathbf{k}) = \varphi_n^*(\mathbf{k})$ . An immediate consequence is that  $n(-\mathbf{k}, t \rightarrow \infty) = n(\mathbf{k}, t \rightarrow \infty)$ , so that the CFS and CFS peaks must be twin peaks with the same amplitude, width and shape. In the presence of the additional filtering, their long-time contrast is  $C_F^\infty = C_B^\infty = \overline{|\varphi_n(\mathbf{k}_0)|^4 / (|\varphi_n(\mathbf{k}_0)|^2)^2} - 1$ , where the average involves states with energy  $\epsilon_n \approx E$ . This value is governed by the statistics of localized wavefunctions  $\varphi_n$  [22, 23]. In the simplest case where the localization length is much larger than the lattice spacing, the Hamiltonian inside a localization volume can be modelled by a random matrix belonging to the Gaussian Orthogonal Ensemble (GOE): the  $\varphi_n(\mathbf{k}_0)$  are then independent random complex Gaussian variables. This leads to

$C_F^\infty = C_B^\infty = 1$  and thus  $\Lambda = 1$ , in agreement with our numerical observations.

In the metallic phase, this reasoning breaks down. Because eigenstates are delocalized over an infinite volume, there is no minimum energy scale in the expansion (2). In other words, Eq. (3) is never valid, even at very long times, and the off-diagonal terms are responsible for the absence of CFS. This makes an interesting connection with the properties of the energy spectrum [30]: pure point dense in the insulating phase, absolutely continuous in the metallic phase.

The behavior at long – but not infinite – time can be also computed from Eq. (2), if we assume that the  $\varphi_n(\mathbf{k})$  and the  $\epsilon_n$  are statistically uncorrelated variables. We can then break the average in Eq. (2) as a product of an average over the  $\varphi_n(\mathbf{k})$  and an average over the  $\epsilon_n$ . The latter average is proportional to the spectral form factor  $K(t)$ , i.e. the Fourier transform of the DOS-DOS correlator  $K(\omega) = \overline{\rho(E + \hbar\omega/2)\rho(E - \hbar\omega/2)}/\rho^2 - 1$  [22, 23]. We thus obtain:

$$C_F(t) = C_F^\infty 2\pi\hbar\rho M^3 K(t). \quad (4)$$

The time scale over which off-diagonal terms vanish in Eq. (2) can be estimated as follows. The average energy spacing between consecutive levels for a system of size  $\xi_{\text{loc}}$  (where  $\xi_{\text{loc}}$  is the localization length) is  $\Delta = \rho\xi_{\text{loc}}^3$ , so that off-diagonal terms will mostly average to zero beyond the Heisenberg time  $\tau_H = 2\pi\hbar/\Delta = 2\pi\hbar\rho\xi_{\text{loc}}^3$ . At times  $t \gg \tau_H$ ,  $K(\omega)$  is obtained by estimating the hybridization of localized states with energies lying within  $\Delta$  [31]. Such an approach has been presented in [23]. A similar calculation in 3D gives  $K(\omega) - \delta(\hbar\rho M^3\omega) \sim (\xi_{\text{loc}}/M)^3 \ln^3(|\omega|\tau_H/4\pi)$  for  $|\omega|\tau_H \ll 1$ . After Fourier transforming this expression with respect to  $\omega$ , we find

$$\Lambda(W, t) \approx 1 - \alpha \frac{\ln^2(\eta t/\tau_H)}{(t/\tau_H)} \quad (W > W_c), \quad (5)$$

where the 1 comes from the  $\delta$  contribution in  $K(\omega)$ . The phenomenological constants  $\alpha$  and  $\eta$  respectively account for subdominant corrections in the distribution of localized states and for a possible numerical prefactor in the definition of  $\tau_H$ . In the insulating phase, we thus predict  $\lim_{t \rightarrow \infty} \Lambda(W, t) = 1$  and, more importantly, that  $\Lambda(W, t)$  should only depend on  $t$  and  $W$  through the ratio  $t/\tau_H$ . This is indeed what is observed in the right panel of Fig. 3, where all numerical points, obtained for different  $W$ , collapse on a single curve in agreement with the theoretical prediction (5) with  $\alpha = 3.72$  and  $\eta = 0.129$ .

This one-parameter scaling can be generalized to the whole range of disorder strengths if one defines a correlation length  $\xi$  such that  $\xi \propto \xi_{\text{loc}}$  in the insulating phase and  $\xi \propto [2\pi\hbar\rho D]^{-1}$  in the metallic one. Indeed, by introducing a “system size”  $L = [t/2\pi\hbar\rho]^{1/3}$  [23], we observe that both Eqs. (1) and (5) depend on  $L/\xi$  only. This suggests that  $\Lambda$  is a natural one-parameter scaling quantity

to study the Anderson MIT. In the spirit of the historical scaling theory of Anderson localization [3], we define a dimensionless “conductance”

$$g(L/\xi) = \Lambda^{-2/3} - 1. \quad (6)$$

This definition gives  $g \approx L/\xi$  in the metallic phase,  $g \rightarrow 0$  in the insulating phase and  $g \approx 1$  at the critical point, very much like the true conductance of a disordered wire. According to the above discussion, the scaling function  $\beta(g) = d(\ln g)/d(\ln L)$  should depend on  $g$  only. This is confirmed in Fig. 4, where points obtained by computing numerically  $\Lambda$  at various times and disorder strengths fall all on the same curve, with the asymptotic limits  $\beta(g \rightarrow \infty) = 1$  and  $\beta(g \rightarrow 0) = -3$  [32]. As time increases, the system goes metallic when  $\beta(g) > 0$  and insulating when  $\beta(g) < 0$ . The critical phase is signaled by the fixed point  $\beta(g) = 0$  (corresponding to the time independence of  $\Lambda(W_c)$  discussed above) and is achieved for  $g \approx 1$ , a value reminiscent of the Thouless criterion [3].

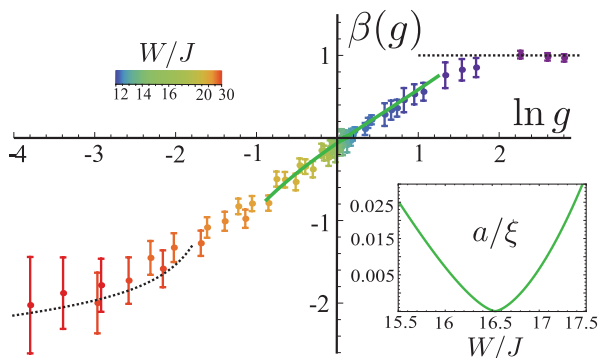


FIG. 4. (Color online) Scaling function  $\beta(g) = d(\ln g)/d(\ln L)$  associated to the dimensionless conductance  $g(L)$  defined in Eq. (6), with  $L = [t/2\pi\hbar\rho(E)]^{1/3}$ . The points are obtained by using data for  $\Lambda$ . Each color corresponds to a value of  $W$  and, for each  $W$ , each point corresponds to a different time  $t$ . All points fall on a single curve. Dotted curves are the asymptotes  $\beta(g \rightarrow \infty)$  and  $\beta(g \rightarrow 0)$  deduced from Eqs. (1) and (5), respectively. The solid curve around  $\beta = 0$  is obtained by a finite-size scaling approach and is used to determine precisely the critical parameters of the transition. The inverse of the correlation length  $\xi$  is shown in the inset.

In the close vicinity of the Anderson MIT, we expect  $D \propto (W_c - W)^\nu$  and  $\xi_{\text{loc}} \propto (W - W_c)^{-\nu}$ , i.e.  $\xi \propto |W - W_c|^{-\nu}$ . To precisely determine the critical parameters  $W_c$  and  $\nu$ , we use a finite-size scaling analysis. It consists in writing  $\Lambda = F(\chi L^{1/\nu})$  with  $|\chi| \propto \xi^{-1/\nu}$  (scaling hypothesis) and fitting the numerical data with a double Taylor expansion  $\Lambda = \sum_{n=0}^{n_R} F_n \chi^n L^{n/\nu}$  and  $\chi = \sum_{m=1}^{m_R} b_m (W - W_c)^m$  where  $F_n$ ,  $b_m$ ,  $W_c$  and  $\nu$  are the fit parameters [29]. With our 1095 data points, we obtain a good fit for  $n_R = m_R = 2$ , achieving a chi-square per degree of freedom  $\approx 1.6$ . The inset of Fig. 4 shows the numerical results obtained for  $1/\xi$  with this approach, which agree very well with an inde-

pendent numerical calculation using the transfer-matrix method [27, 28]. The fitting procedure provides the precise values of the critical point  $W_c = 16.53 \pm 0.03J$ , the critical exponent  $\nu = 1.51 \pm 0.07$ , and the critical contrast  $\Lambda_c = 0.329 \pm 0.010$  [33]. For completeness, we also display in the main panel of Fig. 4 the scaling function  $\beta(g)$  deduced from this analysis close to the critical point (solid curve).

An intriguing question is the physical meaning of  $\Lambda_c \equiv \Lambda(W_c)$ . Since  $\Lambda_c$  is time independent, and assuming that the equality between  $\Lambda$  and the form factor still holds at the critical point, we infer  $\Lambda_c = \lim_{t \rightarrow 0} 2\pi\hbar\rho M^3 K(t) \equiv \kappa(W_c)$ , a positive quantity known as the *spectral compressibility* [34]. It quantifies the fluctuations of the energy spectrum. In the metallic phase, the spectrum is rigid – approximately described by the GOE ensemble of random matrices – fluctuations are small:  $\kappa \rightarrow 0$ . In the insulating phase, fluctuations are large and  $\kappa = 1$ . At the critical point,  $\kappa$  takes on an intermediate value [35] which carries information on the multifractal character of eigenstates at the Anderson MIT. It has been recently conjectured that  $\kappa(W_c) = 1 - D_1/3$ , where the “information dimension”  $D_1$  gives the amount of entropy of the critical eigenstates [36]. For the Anderson model, it is known [37–39] that  $D_1 = 1.97$ , which leads to the prediction  $\Lambda_c = \kappa(W_c) = 0.343$ , in good agreement with the numerically measured value  $\Lambda_c = 0.329 \pm 0.011$ . This demonstrates that the CFS peak at criticality could be used as a direct experimental probe of  $D_1$  [40]. Let us finally note that, in the absence of multifractality, one would have  $D_1 = d = 3$  and thus no CFS at the critical point. In that sense, the critical CFS peak is a direct proof of a multifractal behavior.

In conclusion, we have shown that the CFS interference peak constitutes an experimentally measurable order parameter for the 3D Anderson MIT. The peak contrast obeys the one-parameter scaling hypothesis and provides information on the critical exponents and the multifractal character of eigenstates at the transition. Unlike CBS, CFS is a robust phenomenon which does not seem to require any specific symmetry, and therefore can be used to characterize different types of Anderson MITs beyond the conventional orthogonal symmetry class.

SG acknowledges the support of the PHC Merlion Programme of the French Embassy in Singapore. This work was granted access to the HPC resources of TGCC under the allocations 2015-057083 and 2016-057644 made by GENCI (Grand Equipement National de Calcul Intensif) and to the HPC resources of MesoPSL financed by the Region Ile de France and the project Equip@Meso (reference ANR-10-EQPX-29-01) of the programme Investissements d’Avenir supervised by the Agence Nationale pour la Recherche. This research is supported by the National Research Foundation, Prime Minister’s Office, Singapore and the Ministry of Education, Singapore under the Research Centres of Excellence programme.

- 
- [1] P. W. Anderson, Phys. Rev. **109**, 1492 (1958).
- [2] J. T. Edwards and D. J. Thouless, J. Phys. C **5**, 807 (1972).
- [3] E. Abrahams, P. W. Anderson, D. C. Licciardello, and T. V. Ramakrishnan. Phys. Rev. Lett. **42**, 673 (1979).
- [4] F. Evers and A. D. Mirlin, Rev. Mod. Phys. **80**, 1355 (2008).
- [5] V. Dobrosavljević, N. Trivedi, and J. M. Valles, Jr. (eds.), *Conductor-Insulator Quantum Phase Transitions*, Oxford University Press (2012).
- [6] P. A. Lee and T. V. Ramakrishnan, Rev. Mod. Phys. **57**, 287 (1985).
- [7] S. Katsumoto, F. Komori, N. Sano and S. Kobayashi, J. Phys. Soc. Jap. **56**, 2259 (1987).
- [8] S. Waffenschmidt, C. Pfeiderer, and H. v. Löhneysen, Phys. Rev. Lett. **83**, 3005 (1999).
- [9] H. Hu, A. Strybulevych, J. H. Page, S. E. Skipetrov, B. A. van Tiggelen, Nat. Phys. **4**, 945 (2008).
- [10] A. Aubry, L. A. Cobus, S. E. Skipetrov, B. A. van Tiggelen, A. Derode, and J. H. Page, Phys. Rev. Lett. **112**, 043903 (2014).
- [11] L. A. Cobus, S. E. Skipetrov, A. Aubry, B. A. van Tiggelen, A. Derode, and J. H. Page, Phys. Rev. Lett. **116**, 193901 (2016).
- [12] J. Chabé, G. Lemarié, B. Grémaud, D. Delande, P. Szriftgiser, and J. C. Garreau, Phys. Rev. Lett. **101**, 255702 (2008).
- [13] F. Jendrzejewski, A. Bernard, K. Müller, P. Cheinet, V. Josse, M. Piraud, L. Pezzé, L. Sanchez-Palencia, A. Aspect, and P. Bouyer, Nat. Phys. **8**, 398 (2012).
- [14] G. Semeghini, M. Landini, P. Castilho, S. Roy, G. Spagnolli, A. Trenkwalder, M. Fattori, M. Inguscio, and G. Modugno, Nat. Phys. **11**, 554 (2015).
- [15] D. Delande and G. Orso, Phys. Rev. Lett. **113**, 060601 (2014).
- [16] A. D. Mirlin, F. Evers, I. V. Gornyi, and P. M. Ostrovsky Int. J. of Mod. Phys. B **24**, 1577 (2010).
- [17] S. Faez, A. Lagendijk, A. Strybulevych, J. H. Page, and B. A. van Tiggelen, Phys. Rev. Lett. **103**, 155703 (2009).
- [18] D. S. Wiersma, P. Bartolini, Ad Lagendijk, and R. Righini, Nature **390**, 671 (1997).
- [19] A. A. Chabanov, M. Stoytchev, A. Z. Genack, Nature **404**, 850 (2000).
- [20] T. Sperling, L. Schertel, M. Ackermann, G.J. Aubry, C.M. Aegerter and G Maret, New J. Phys. **18**, 013039 (2016).
- [21] T. Karpiuk, N. Cherroret, K. L. Lee, B. Grémaud, C. A. Müller, and C. Miniatura, Phys. Rev. Lett. **109**, 190601 (2012).
- [22] K. L. Lee, B. Grémaud and C. Miniatura, Phys. Rev. A **90**, 043605 (2014).
- [23] S. Ghosh, N. Cherroret, B. Grémaud, C. Miniatura, and D. Delande, Phys. Rev. A **90**, 063602 (2014).
- [24] The temporal dependence of the width of the CBS peak can also be used to locate the Anderson transitions [29].
- [25] B. A. van Tiggelen and R. Maynard, in *Wave Propagation in Complex Media* (pp. 247-271), Springer, New York (1998).
- [26] T. Micklitz, C. A. Müller, and A. Altland, Phys. Rev. Lett. **112**, 110602 (2014).
- [27] B. Kramer and A. MacKinnon, Rep. Prog. Phys. **56**, 1269 (1993).
- [28] K. Slevin and T. Ohtsuki, New J. Phys. **16**, 015012 (2014).
- [29] S. Ghosh, D. Delande, C. Miniatura, and N. Cherroret, Phys. Rev. Lett. **115**, 200602 (2015).
- [30] R. Carmona and J. Lacroix, *Spectral Theory of Random Schrödinger Operators*, Birkhäuser Boston (Cambridge MA, 1990).
- [31] N. F. Mott, Philos. Mag. **2**, 7 (1970).
- [32] The behavior of  $\beta(g)$  at vanishingly small  $g$  is slightly different from the one of the conductance of a disordered wire where  $\beta \rightarrow -\infty$ , but similar to what is observed in other systems, see [41] or the  $\chi$  function in [42].
- [33] To extract the uncertainties, we proceed as in [29]: we divide the whole configuration sample into several independent subsets and estimate  $W_c$ ,  $\nu$  and  $\Lambda_c$  for each subset.
- [34] J. T. Chalker, I. V. Lerner, and R. S. Smith, Phys. Rev. Lett. **77**, 554 (1996); J. Math. Phys. **37**, 5061 (1996).
- [35] I. K. Zharekeshev and B. Kramer, Jpn J. Appl. Phys. **34**, 4361 (1995).
- [36] E. Bogomolny and O. Giraud, Phys. Rev. Lett. **106**, 044101 (2011).
- [37] In 3D, the  $2 + \epsilon$  perturbation expansion provides  $D_1 = 2$  and  $D_2 = 1$  [4].
- [38] A. Rodriguez, L. J. Vasquez, and R. A. Römer, Phys. Rev. B **78**, 195107-9 (2008).
- [39] The value  $D_1 = 1.971 \pm 0.003$  can be extracted by interpolating the data presented for  $D_q$  in *High-precision multifractal analysis in the 3D Anderson model of localisation*, L. J. Vasquez, PhD thesis, University of Warwick (2010), unpublished. The same reference gives  $D_2 = 1.243 \pm 0.006$ .
- [40] The alternate conjecture  $2\kappa = 1 - D_2/3$  [43] predicts  $\kappa \approx 0.29$ , significantly deviating from our numerical results.
- [41] G. Lemarié, J. Chabé, P. Szriftgiser, J.C. Garreau, B. Grémaud and D. Delande, Phys. Rev. A **80**, 043626 (2009).
- [42] A. MacKinnon and B. Kramer, Z. Phys. B **53**, 1 (1983).
- [43] J. T. Chalker, V. E. Kravstov and I. V. Lerner, JETP Lett. **64**, 386 (1996).